J Physiol 588.24 (2010) pp 4969–4985

The Journal of Physiology

Mechanosensitivity of $Na_v1.5$, a voltage-sensitive sodium channel

Arthur Beyder[1], James L. Rae[1], Cheryl Bernard[1], Peter R. Strege[1], Frederick Sachs[2] and Gianrico Farrugia[1]

[1] *Enteric Neuroscience Program, Mayo Clinic, Rochester, MN, USA*
[2] *Center for Single Molecule Biophysics, Physiology and Biophysical Sciences, University at Buffalo, State University of New York, Buffalo, NY, USA*

The voltage-sensitive sodium channel $Na_v1.5$ (encoded by *SCN5A*) is expressed in electro-mechanical organs and is mechanosensitive. This study aimed to determine the mechano-sensitive transitions of $Na_v1.5$ at the molecular level. $Na_v1.5$ was expressed in HEK 293 cells and mechanosensitivity was studied in cell-attached patches. Patch pressure up to −50 mmHg produced increases in current and large hyperpolarizing shifts of voltage dependence with graded shifts of half-activation and half-inactivation voltages ($\Delta V_{1/2}$) by ∼0.7 mV mmHg^{-1}. Voltage dependence shifts affected channel kinetics by a single constant. This suggested that stretch accelerated only one of the activation transitions. Stretch accelerated voltage sensor movement, but not rate constants for gate opening and fast inactivation. Stretch also appeared to stabilize the inactivated states, since recovery from inactivation was slowed with stretch. Unitary conductance and maximum open probability were unaffected by stretch, but peak current was increased due to an increased number of active channels. Stretch effects were partially reversible, but recovery following a single stretch cycle required minutes. These data suggest that mechanical activation of $Na_v1.5$ results in dose-dependent voltage dependence shifts of activation and inactivation due to mechanical modulation of the voltage sensors.

(Received 17 September 2010; accepted after revision 27 October 2010; first published online 1 November 2010)
Corresponding author G. Farrugia: Mayo Clinic, 200 First Street SW, Rochester, MN 55905, USA.
Email: farrugia.gianrico@mayo.edu

Abbreviations CSI, closed state inactivation; SF, scaling factor.

Introduction

Voltage-sensitive ion channels may also be mechanosensitive

Voltage-sensitive ion channels are nano-machines that serve as biological transistors with well-defined primary functions (Hille, 2001). Many voltage-sensitive ion channels are expressed in contractile organs, which prompted consideration of mechanical modulation of ion channel function. The mechanosensitivity of voltage-sensitive sodium-selective ion channels (Na_v channels) was first noted in mechanically manipulated *Loligo* nerve fibres, where an increase in hydro-static pressure depolarized the membrane potential and decreased the amplitude of the action potential (Baker *et al.* 1962). Since the advent of molecular cloning, the list of eukaryotic voltage-sensitive ion channels that are also mechanosensitive has grown. These include representatives from the families of calcium (Farrugia *et al.* 1999; Calabrese *et al.* 2002; Kraichely *et al.* 2009), potassium (Gu *et al.* 2001; Laitko & Morris, 2004) and sodium (Tabarean *et al.* 1999; Ou *et al.* 2003; Morris & Juranka, 2007; Wang *et al.* 2009) channels.

The mechanosensitivity of voltage-sensitive channels is not surprising, as the conformational rearrangements required for both sensing the voltage (Schmidt & Mackinnon, 2008) and for gating involve physical changes in the shape of the channel (Zhao *et al.* 2004). The conformational states undergone by the channel during the gating process have various sizes and shapes, and any of these transitions could be mechanosensitive (Gu *et al.* 2001; Calabrese *et al.* 2002; Strege *et al.* 2003*a*; Laitko & Morris, 2004; Laitko *et al.* 2006; Morris & Juranka, 2007; Kraichely *et al.* 2009). The mechanosensitivity can also be influenced by the channel environment. Most notably, crystallographic data suggest that the voltage sensors lie at the periphery of the channel and interact with the boundary lipids (Jiang *et al.* 2003; Milescu *et al.* 2009). Therefore, an emerging concept is that the function of the voltage sensors is modulated by the surrounding lipids. In turn, channel gating also impacts the structural and

DOI: 10.1113/jphysiol.2010.199034

mechanical states of the bilayer (Schmidt & Mackinnon, 2008; Beyder & Sachs, 2009; Kraichely *et al.* 2009; Milescu *et al.* 2009).

Voltage-sensitive sodium selective ion channels are mechanosensitive

Mechano-regulation of Na_v channels in electromechanical tissues is of particular interest. Given the steep voltage sensitivity of these channels, even small changes in channel kinetics can affect physiology. Two laboratories have demonstrated the mechanosensitivity of a rat muscle Na^+ channel, $Na_v1.4$ (SkM1) (Shcherbatko *et al.* 1999; Tabarean *et al.* 1999). Both studies showed irreversible changes in steady-state and transient kinetic parameters as a result of patch suction in cell-attached patches of *Xenopus* oocytes expressing $Na_v1.4$ (Tabarean *et al.* 1999). Suction of 30 mmHg induced a large (−20 mV) shift in the voltage dependence of steady-state activation and inactivation. Moreover, the channels in the patch underwent a permanent conversion from predominately 'slow' to 'fast' kinetics of activation and inactivation. As these effects were irreversible, the authors hypothesized an involvement of the cytoskeleton. They showed that patch excision and microtubule disruption accelerated the shift to the 'fast' kinetics mode. Shcherbatko *et al.* (1999) extended their study to the peripheral nerve sodium channel $Na_v1.7$ (PN1) with similar results. Recently, $Na_v1.6$, localized at the axonal nodes of Ranvier, was found to have a similar irreversible hyperpolarizing shift in voltage dependence in response to mechanical stimulation (Wang *et al.* 2009).

$Na_v1.5$ is a voltage-sensitive sodium channel found in two human electromechanical systems, the heart (Gellens *et al.* 1992) and the gut (Lyford & Farrugia, 2003). Mutations in $Na_v1.5$ result in disease. In the heart, $Na_v1.5$ mutations are known to cause long QT 3 (LQT3), Brugada syndrome, cardiac conduction disease and dilated cardiomyopathy (Bennett *et al.* 1995; Ackerman, 1998). In the gut, mutations in $Na_v1.5$ are associated with an increased incidence of abdominal pain syndromes (Locke *et al.* 2006). It also appears that mechanical sensitivity of $Na_v1.5$ may play a role in pathophysiology of irritable bowel syndrome. Recently, a mutant $Na_v1.5$ (G298S) from a patient with irritable bowel syndrome was found to be less responsive to shear stress than wild-type $Na_v1.5$ (Saito *et al.* 2009).

In both the heart and gut, there is continual oscillating movement, making the effect of mechanical stress particularly relevant. We and others have demonstrated mechanosensitivity of $Na_v1.5$ on a macroscopic level (Strege *et al.* 2003*b*; Morris & Juranka, 2007). For $Na_v1.5$ channels expressed in HEK cells, shear stress increased peak current by 27% and accelerated activation (Strege *et al.* 2003*a*). Later, in *Xenopus* oocyte cell-attached patches, Morris & Juranka (2007) showed that suction produced a reversible 40% acceleration of $Na_v1.5$ activation and inactivation. This suggested a small negative shift in midpoints of ∼2–4 mV. A subsequent study found a more significant shift of 10 mV for −30 mmHg (Banderali *et al.* 2010). The authors also examined stretch effects on two LQT3 $Na_v1.5$ mutants (R1623Q and R1626P). As these mutant channels have previously been shown to have uncoupled activation and inactivation, it was surprising that stretch did not have a differential effect on the activation and inactivation of the channels. These studies have established stretch sensitivity of $Na_v1.5$. However, the precise effects of stretch on the specific gating transitions remain unclear.

A kinetic model of Na_v channels is complex

To understand the effects of stretch on rate constants requires that mechanical effects be considered with respect to the effects of stretch on discrete gating transitions. Previous studies on whole cells and cell-attached patches yielded large macroscopic currents (Shcherbatko *et al.* 1999; Tabarean *et al.* 1999; Morris & Juranka, 2007). These demonstrated mechanical modulation of Na_v and specifically $Na_v1.5$, but these studies lacked single channel data and detailed analysis of the distinct transitions in the Na_v gating scheme. Our aim was to characterize the mechanosensitivity of Na_v channels by determining the stretch-dependent transitions. A practical difficulty is that Na_v channels have complex kinetic properties, and while multiple models have been proposed, a consensus kinetic model does not exist (Armstrong & Bezanilla, 1977; Bezanilla & Armstrong, 1977; Armstrong, 2006). In order to better understand which gating transitions are mechanosensitive we examined mechanosensitivity using a highly simplified five state model. This model simply outlines the widely accepted gating transitions of the Na_v channels (Fig. 1). At rest (hyperpolarized), the voltage-sensitive Na^+ channel is closed (state C) and the voltage sensors are in the rest position. A depolarization activates the channels via a series of voltage-dependent steps, but will be denoted here by a single step $C \rightarrow C_A$ with q representing voltage dependence. From the activated state, the channel can proceed to an open and conducting state via a *voltage-independent* transition ($C_A \rightarrow O$). Inactivation may occur from both the open (O) and the activated (C_A) states. When a large depolarization drives all channels to activation, opening of the cytoplasmic ion channel gate makes the inactivation site accessible and allows the inactivation particle to quickly close the channel ($O \rightarrow I_O$). At potentials negative with respect to channel opening, channels may enter the inactivated state directly from the activated (C_A)

state without opening, also called closed state inactivation ($C_A \rightarrow I_A$). Recovery from the inactivated states (I_A and I_O) is followed by the voltage sensors returning to their deactivated position ($C_A \rightarrow C$). In this study, we examined the effects of mechanical perturbations on the specific transitions in this gating scheme.

We used $Na_v1.5$-transfected HEK cells and stretched cell-attached patches. A single stretch of the membrane caused a persistent increase in current and hyperpolarizing shifts in the midpoint of activation and inactivation. We show that the shifts in voltage dependence were due to an acceleration of a single voltage sensing step. Channel gate function, inactivation from open states (fast inactivation), and unitary conductance were unaffected by stretch. Stretch slowed recovery from inactivation, suggesting that the inactivated states were stabilized. These data also suggest that mechanosensitivity of $Na_v1.5$ may play a significant role in the behaviour of the channel in mechanically active organs.

Methods

Pipette fabrication

Patch pipettes were pulled from 2.7-inch length Corning 7040 glass tubing (Corning Inc., Corning, NY, USA; 1.65 mm OD, 1.15 mm ID), using a four stage pull by a Sutter P-97 electrode puller (Sutter Instrument Co., Novato, CA, USA). The tips were intentionally pulled to be blunt (bullet-nosed). After pulling, the final tip geometry was achieved by fire polishing. In general, fire polishing was done at higher than normal temperature with the tip farther from the glass coated filament than customary for construction of low noise pipettes. These procedures produced a rounding of the tip without much narrowing of the internal diameter. The final tip diameter could be controlled by adjusting the duration of fire polishing. Several iterative experiments with different tip geometries allowed the desired recordings in about half of the patches. In addition, the selected tip geometry produced patches that were consistently sensitive to patch pressure.

Cell culture

Human embryonic kidney cells 293 (HEK) (American Type Culture Collection, Manassas, VA, USA) were grown in T25 flasks in minimum essential medium, 10% horse serum, non-essential amino acids, sodium pyruvate and penicillin–streptomycin (Invitrogen, Carlsbad, CA, USA). Cells were grown to about 75% confluency. One day prior to the experiments, flasks were transfected with *SCN5A* encoding the hH1C3 variant (the most prevalent variant in the gut; Strege and others 2003*b*), and with green fluorescent protein (GFP) pEGFP-C1 (Clontech, Palo Alto, CA, USA), using Lipofectamine 2000 reagent and OPTI-MEM I reduced serum medium (Invitrogen) (Saito and others 2009). On the morning of the experiments, cells were trypsinized and resuspended in Ringer solution, and plated onto the recording chamber 15 min prior to the initiation of experiments.

Recording solutions

The bath solution contained (in mM): 149.2 Na^+, 159 Cl^-, 4.7 K^+, 2.5 Ca^{2+}, and 5.0 Hepes (and 5.5 mM glucose for the whole cell experiments). Pipette solution was made of bath solution plus 10 μM $GdCl_3$ to minimize contamination by endogenous cation selective stretch channels (Morris *et al.* 2006). The bath solution was made in bulk, but gadolinium solution was prepared on the day of the experiments. Since use of gadolinium (Caldwell *et al.* 1998) has been shown to affect Na_v channels (Elinder & Arhem, 1994), we determined the minimal amount required. The addition of 10 μM $GdCl_3$ to the pipette solution was sufficient in blocking endogenous cation-selective stretch currents (Fig. S1 in the online Supplemental Material). For whole cell experiments, the intracellular (pipette) solution was (in mM): 135 K^+, 130 $CH_3SO_3^-$, 5 Na^+, 5 Mg^{2+}, 5 Hepes, and 2 EGTA in the tip with 0.6 mM amphotericin B added to the backfill (final DMSO concentration was less than 1%).

Mechanical stimuli

Transfected cells were identified by fluorescence microscopy, and cell-attached patches were formed using standard techniques. Gentle suction was applied to make a gigaseal and patch pressure was then released. Seal history is important for such experiments (Morris *et al.* 2006), therefore we recorded the pressures required for patch formation. Patches were typically formed at <5 mmHg.

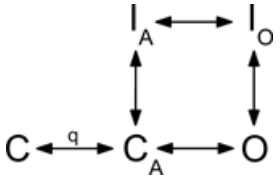

Figure 1. Simplified Na_v gating model
In the resting state all channels are in state C. With depolarization, channels proceed through the voltage-dependent (q) states, as the four voltage sensors move into the activated positions. From this activated state (C_A), channels may either proceed to inactivation ($C_A \rightarrow I_A$) or to the open state (O). The transition to the open conducting state ($C_A \rightarrow O$) is independent of voltage, representing opening of the intracellular gate. Shortly after opening, the channel is inactivated by an intracellular inactivation gate ($O \rightarrow I_O$). Recovery from the inactivated states may proceed without channel opening, so $I_O \rightarrow I_A \rightarrow C_A$.

Patches with seals that were formed at >10 mmHg were discarded. Pressure was stepped to the desired level for a few seconds prior to protocol execution, and then stepped back to 0 mmHg between successive datasets.

A significant impediment to studying the mechanosensitivity of ion channels is the inability to apply a precise mechanical stimulus. Mechanical stress is difficult to apply reproducibly and hence local stress is often ill-defined. For experimental systems that aim to combine voltage- and mechano-clamp, application of pressure to a voltage-clamped membrane patch is the most reproducible stimulus available (Suchyna *et al.* 2009). Patch pressure was modulated with a pneumatic transducer (DPM-1, Bio-Tek, Winooski, VT, USA). Determination of the actual stimulus at the patch is complicated because the geometry is not spherical, and the patch anatomy is inhomogeneous and changing in time (Suchyna *et al.* 2009). Therefore, we focused on differential effects within the same patch (Opsahl & Webb, 1994). Video recordings demonstrated patch creep at suction greater than −30 mmHg (Fig. S2). We performed experiments at pressures as high as −120 mmHg, but due to patch creep most of the quantitative analysis was from 0 and −30 mmHg. To minimize drift caused by time-dependent changes in the patch properties (Morris *et al.* 2006), we limited the data acquisition to 30 seconds at elevated pressure.

Electrophysiology

An Axopatch 200A amplifier, Digidata 1322A, and Clampex 9.0 software (Molecular Devices, Sunnyvale, CA, USA) were used for voltage-clamp and data acquisition. Previous work showed that large transmembrane voltages (100+ mV) applied over seconds produced patch creep, which caused activation of mechanosensitive channels in *Xenopus* oocytes (Gil *et al.* 1999). To prevent this creep, we kept the holding potential at 0 mV.

Average current data collection & analysis

The fast inactivation of Nav1.5 channels is complete in only a few milliseconds, but recovery requires hundreds of milliseconds at a holding potential of −100 mV (Bezanilla & Armstrong, 1977). However, channels can be more rapidly restored by a strong hyperpolarization (Bezanilla & Armstrong, 1977). We found that full recovery from inactivation can be accomplished within a few milliseconds ($\tau = 0.59$ ms) using short (2–5 ms) hyperpolarizing pulses to −204 mV (maximum functional range of our amplifier) (Fig. S3). By minimizing intersweep intervals, we were able to acquire sufficient single channel events over a 30 s period at elevated pressure. $P/4$ subtraction was used to minimize capacity transients (holding potential (HP) = 0 mV).

Average traces resembled macroscopic currents and were treated as such. We used Origin 7.0 (OriginLab Co., Northampton, MA, USA) to fit normalized peak currents (I/I_{max}) that were plotted against applied voltage using a two state Boltzmann model ($I/I_{max} = A/[1 + \exp((V_{1/2} - V)/dV)]$), where I is current, I_{max} is maximal current, A is a scaling factor, $V_{1/2}$ is the voltage at half-maximal current, and dV is the slope of the sigmoidal gating curve.

Single channel data collection and analysis

A sequence of 200–1000 steps maximized the number of events while keeping the protocol time to approximately 30 s. A separate protocol to $P/4$ (HP = 0 mV) was acquired after each sequence and was scaled and subtracted offline. Data were analysed in QuB, a freely available software package (www.qub.buffalo.edu). The data were filtered at 2 kHz and single channel events were idealized using the SKM routine with baseline levels fixed and optimized using log likelihood (Qin *et al.* 1996; Qin, 2004). Events were indexed and exported to Origin 7.0, where data were analysed statistically. The number of open channels in the patch was assumed to obey a binomial distribution of the total number (Horn, 1991). If the number of channels in the patch is n, and the open probability is P_o, then for a number of sweeps m, the probability (k) that the maximum observed level is the total number of channels in the patch is $k = 1 - (1 - P_o^n)^m$. Since activation and inactivation overlap temporally the maximum P_o is less than 1.0 and is difficult to estimate. To estimate the maximum P_o and to count the number of channels in the patch, we used patches with a small number of channels ($n < 10$), and depolarized them to (0, +5 and +10 mV), where P_o should be maximal and acquired $m = 600$ sweeps. Under these conditions, we could count up to five channels with greater than 90% confidence ($k > 0.9$) for $P_o > 0.3$. P_o at peak current was calculated from a single sweep using $P_o = I_{avg}/I_{peak}$.

Results

Membrane stretch increases peak current and accelerates both activation and inactivation

Average currents in response to a typical voltage ladder protocol (Fig. 2*A*) for a single patch at 0 mmHg and −30 mmHg are shown in Fig. 2*B* and *C*. To bring channels out of inactivation, we used a 5 ms pulse to maximum hyperpolarization allowed by the amplifier (−204 mV) (Fig. S3). This allowed satisfactory averaging of currents as small as 3 pA over the 30 s stretch steps.

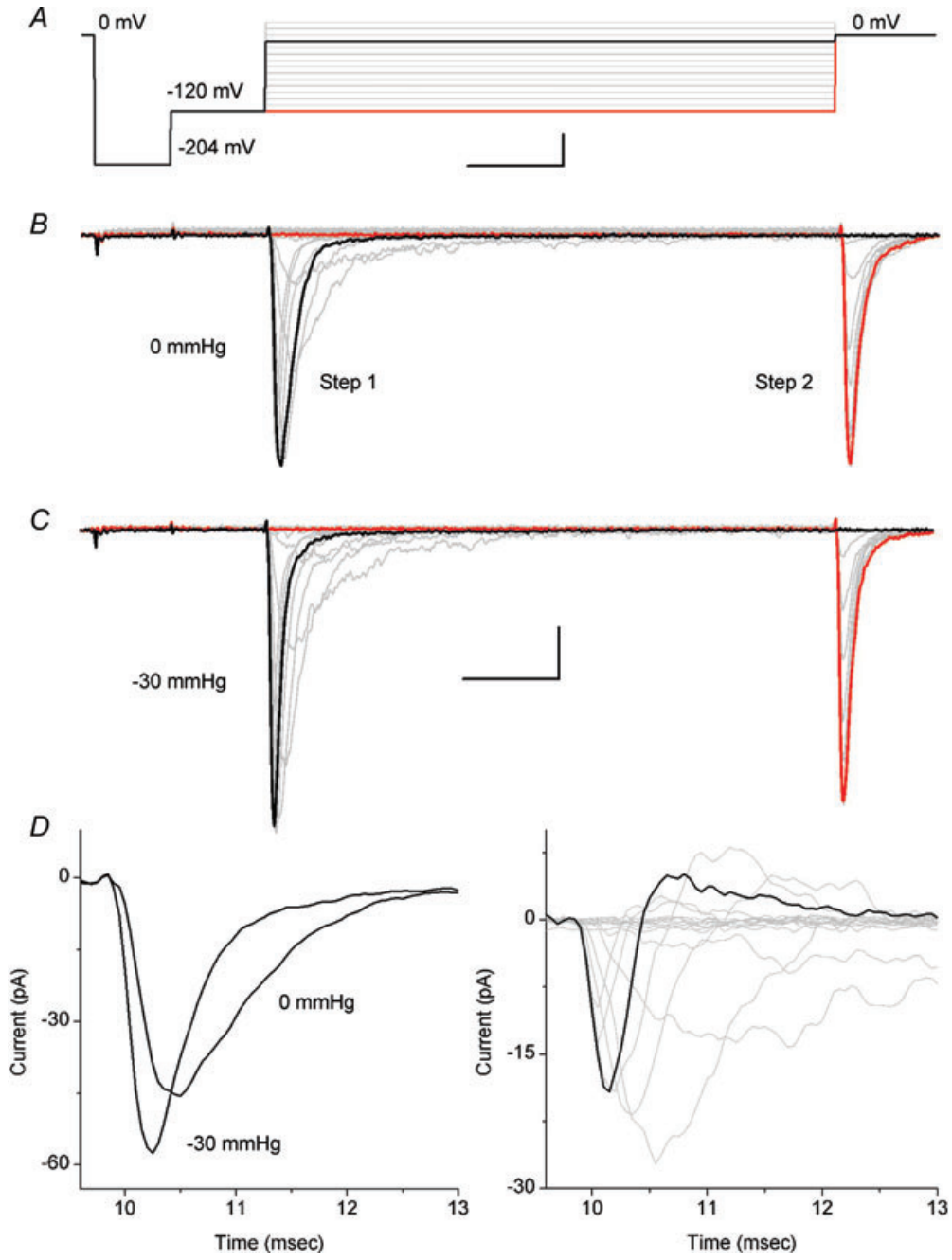

Figure 2. Averaged patch currents increase in peak and accelerate with stretch
A, a typical voltage protocol. From holding potential (0 mV), each 30 ms-long ladder step (starting from −120 to 20 mV in 10 mV increments) was preceded by 5 ms hyperpolarizing pulses to −204 mV and −120 mV (scale 5 ms and 50 mV). Ten averages were obtained for each averaged current experiment. *B* and *C*, average patch current at rest (0 mmHg) (*B*) and average patch current when stretched by a −30 mmHg stimulus (*C*). Peak currents evoked at the beginning of each ladder step (Step 1) and immediately after stepping to 0 mV at the end of each ladder step (Step 2) were used to analyse voltage dependence of activation and inactivation, respectively. For Step 1 black traces show patch currents in response to a depolarization to −10 mV. For Step 2 black traces show no current at 0 mV after a 'prepulse' of −10 mV, and red traces show current at 0 mV after a 'prepulse' to −120 mV. For *B* and *C* scale is 5 ms and 10 pA. *D*, left panel highlights the early portion of Step 1 currents at 0 and −30 mmHg for a depolarization to −10 mV. These traces clearly demonstrate that peak currents increased with stretch and showed accelerated kinetics. The right panel shows the difference in Step 1 currents from left panel (black) and at all voltages (grey) ($I(t)_{0\ \mathrm{mmHg}} - I(t)_{-30\ \mathrm{mmHg}}$).

At 0 mmHg, the average peak current of Step 1 was 47 ± 24 pA (Fig. 2*B*). Patch pressure produced a robust increase in the peak value (Fig. 2*B–D*). At -30 mmHg, for 8 of 10 patches examined Step 1 peak currents increased 33% to 63 ± 29 pA ($n = 10$) (Fig. 2*C*). Suction increased peak currents significantly for -20, -30 and -40 mmHg by 1.32 ± 0.21, 1.33 ± 0.27 and 1.37 ± 0.34, respectively ($n = 6$, $P < 0.05$ compared with 0 mmHg, $P > 0.05$ between pressures). Peak currents for -10 mmHg and -50 mmHg increased but did not reach statistical significance. At low suction (-10 mmHg) the mechanical stimulus was likely to have been too small relative to background variations while at -50 mmHg patch creep may have changed patch properties (Fig. S2). Positive pressure also caused an increase in current (data not shown), showing that membrane tension and not applied pressure was the key variable.

Stretch also had effects on the kinetics of activation and inactivation. For the traces highlighted in black (depolarization to -10 mV) in Fig. 2*B* and *C*, pressure accelerated the time to reach peak current (activation) from 0.49 ms to 0.64 ms (30%) (Fig. 2*D*, left panel). Fast inactivation, which was estimated from the kinetics of current decay from peak current, was also accelerated. When inactivation was fitted to a single exponential, the time constant decreased (accelerated) with stretch from 0.81 to 0.68 ms (29%). The difference in time dependence of current with stretch demonstrated a mix of excitatory effects at small depolarizations (near resting potential) and transient excitatory mixed with later inhibitory effects of large depolarizations at large depolarizations (Fig. 2*D*, right panel).

Stretch left-shifts voltage dependence of steady state activation and inactivation

The voltage ladder protocol shown in Fig. 2*A* was used to assess the macroscopic behaviour for voltage dependence of activation and steady-state inactivation. Voltage dependence of activation was measured as peak currents evoked at the beginning of each ladder step (Step 1 peak). Steady-state inactivation, or availability, was measured as peak currents immediately after stepping to 0 mV at the end of each ladder step (Step 2 peak). These results are qualitatively similar to the macroscopic (whole cell) data (Makielski *et al.* 2003). Mean current–voltage (*I–V*) curves for a typical experiment show that pressure induced a significant shift in the steady-state voltage dependence of activation and inactivation (Fig. 3*A* and *B*). When fitted to a two state Boltzmann model, at 0 mmHg the half-point of activation ($V_{1/2}$) was -33 ± 9 mV ($R = 1.0$) with a slope (dV) of 5.6 ± 0.3 mV ($R = 0.91$) ($n = 6$). $V_{1/2}$ compared well to previous experiments with whole cell currents where $V_{1/2}$ was reported as -40 ± 2 mV and $dV = 4.9 \pm 0.3$ mV (Makielski *et al.* 2003). The wide range of $V_{1/2}$ values in cell-attached experiments was likely due to variable resting potential and tension (Suchyna *et al.* 2009). To quantify voltage errors secondary to the resting potential of the cell we measured the resting potential of HEK cells transfected with $Na_v1.5$. First, a gigaohm seal was established, and amphotericin was allowed sufficient time to perforate the patch. Then, resting voltage was recorded in current clamp mode (0 pA injected). Resting voltage of these cells was -8.1 ± 4.1 mV ($n = 7$).

To minimize the effects of patch to patch variation on our data, we analysed individual patches and compared the relative effects. From tension at rest (0 mmHg applied to patch), we applied pressure stimuli as short 30 s steps with steps back to resting tension in between stimuli. When compared to resting tension, in all 10 of 10 stretched patches, mean current–voltage (*I–V*) curves (Fig. 3) showed a significant shift in the steady state voltage dependence of activation and inactivation. In the voltage range tested (-10 to -50 mmHg), suction-driven shifts of $V_{1/2}$ in Fig. 3 were linear with pressure ($R = 0.97$, $R = 0.99$, respectively) and in the hyperpolarized direction by -0.72 ± 0.18 mV mmHg^{-1} ($n = 4$) for activation and -0.68 ± 0.28 mV mmHg^{-1} for inactivation ($n = 4$) (Fig. 3C). Shifts in half-point of activation were similar when patches were stepped to -30 mmHg in a single step (-19.0 ± 8.2 mV, $n = 6$) or after a couple of increasing steps of increasing pressure (-23.1 ± 6.5 mV, $n = 4$). Boltzmann slopes (dV) showed a trend toward steeper activation but this was not statistically significant at any of the pressures tested ($\Delta dV = 0.022 \pm 0.035$ mV mmHg^{-1} ($n = 4$) for activation and -0.0038 ± 0.041 mV mmHg^{-1} ($n = 4$) for inactivation) (Fig. 3*D*).

The small area below the intersection of the activation and inactivation curves is known as the window current (Fig. 3, inset). Over this voltage range, the activated channels would not be fully driven to inactivation, resulting in a steady-state current. The larger the window, the more significant is the steady-state current. The significance of the window current is enhanced if it is found over the resting voltage of the cell. We show above that stretch resulted in a leftward shift in voltage dependence of activation and inactivation, hence the window current (Fig. 3, inset). However, since the activation and inactivation were similarly affected and there was no significant change in the steepness of the Boltzmann fit, the size of the shifted window current was relatively conserved.

Positive pressure was applied to rule out effects secondary to patch curvature. It produced shifts in voltage dependence with independence of slope sensitivity similar to those observed with negative pressures (Fig. S4). The correlation of positive and negative pressure results implies that the effects were due to membrane tension (Fig. S4). However, negative pressure was more robust

experimentally, and was thus used for the following experiments.

Effect of membrane stretch on activation and fast-inactivation kinetics

The currents in Fig. 2 qualitatively demonstrate an increased rate of activation and inactivation that was typically seen. The activation mechanism of sodium channels is a multi-step process. Facilitation of either the voltage sensor activation (Borjesson *et al.* 2008) or gate opening (Zhao *et al.* 2004) may left-shift activation $V_{1/2}$ and thus produce apparent acceleration of current activation at all voltages. Furthermore, it is known that Na_v activation is kinetically linked to inactivation, because it is fast and rate-limiting (Aldrich *et al.* 1983). Thus, acceleration of activation may also accelerate inactivation. In the next set of experiments, we examined (1) whether or not activation and inactivation are both stretch sensitive and (2) which of the activation processes (voltage sensors or gate opening) are affected by stretch.

The left panel of Fig. 4 shows the *I–V* curves for a typical experiment for a patch at rest (black) and stretched by −30 mmHg (red). The *I–V* curves demonstrate the

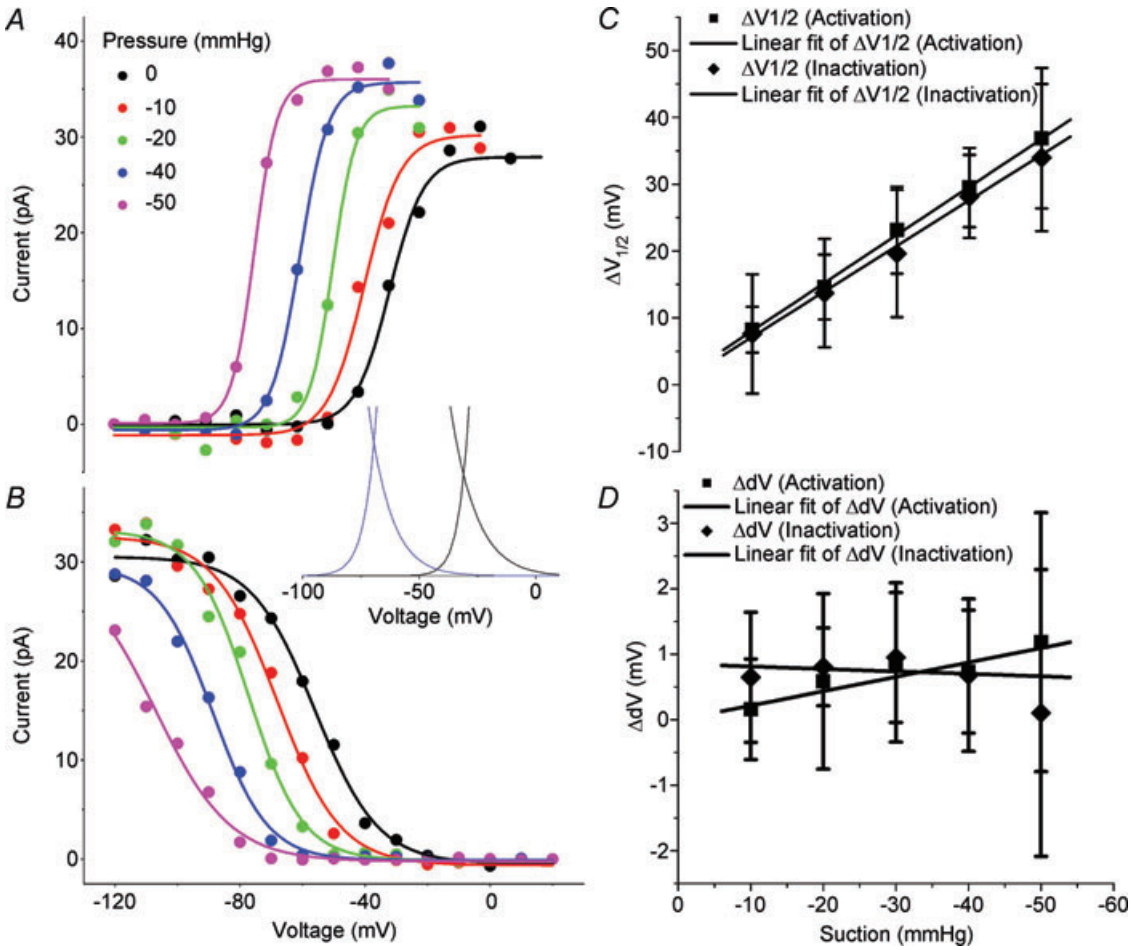

Figure 3. Suction effects on voltage dependence of $Na_v1.5$ activation and inactivation showing a marked leftward shift

A, Two state Boltzmann model fits of voltage dependence of activation at pressures 0 mmHg to −50 mmHg. *B*, Two state Boltzmann model fits of steady-state voltage dependence of inactivation at pressures 0 mmHg to −50 mmHg. Inset shows window currents resulting from overlap of the voltage dependence of activation and inactivation at 0 mmHg and at −40 mmHg showing the leftward shift in the window current with suction. *C*, shift in half-point ($\Delta V_{1/2}$) of activation (squares) and inactivation (diamonds) ($\Delta V_{1/2} = V_{1/2,0\ mmHg} - V_{1/2,testP}$) with response to increasing amplitude suction stimuli from −10 to −50 mmHg. Linear fits of the shift in activation and inactivation were -0.72 ± 0.18 mV mmHg^{-1} ($R = 0.97$) and -0.68 ± 0.28 mV mmHg^{-1} ($R = 0.99$), respectively. *D*, shift in slope (ΔdV) of activation (squares) and inactivation (diamonds) ($\Delta dV = dV_{1/2,0\ mmHg} - dV_{1/2,testP}$) with response to increasing amplitude suction stimuli from −10 to −50 mmHg. Linear fits of the Boltzmann slope of activation and inactivation were 0.022 ± 0.035 mV mmHg^{-1} ($R = 0.30$) and -0.0038 ± 0.041 mV mmHg^{-1} ($R = 0.24$), respectively.

negative shift of voltage dependence of channel activation and the increase in peak current with stretch. Points 1–5 (V_m from −60 mV to −10 mV) were picked along the steep portion of the *I–V* curve where channels are most sensitive to voltage. The traces in the middle panel show the time course of activation and inactivation for currents at these voltages. Stretch increased the peak current and accelerated both activation and inactivation kinetics at all voltages. In the right panel we have normalized peaks to amplitude and time. Temporal scaling was accomplished simply by $t_{scaled} = t/SF$, where the scaling factor (SF) with, $SF = t_{peak,0\ mmHg}/t_{peak,30\ mmHg}$. It is evident from the right panel of Fig. 4 that all traces could be well overlapped using a single linear scaling constant (SF). We performed this analysis in five patches and had good overlap in each case. As a result, it is evident that a single time scaling constant accounted for the complex kinetic changes.

Our data suggest that stretch accelerates activation and inactivation by a single constant. Given the kinetic link between activation and inactivation, it is most likely that stretch produces an acceleration of channel activation, and inactivation only appears faster. Furthermore, the fact that acceleration is explained by simple linear scaling suggests that either the voltage sensor activation step ($C \rightarrow C_A$) or gate opening step ($C_A \rightarrow O$) is affected, but not both.

Inactivation from closed states is enhanced by stretch

Because the kinetics are fast, it was difficult to determine which transitions were affected by stretch: was it activation ($C \rightarrow C_A$) or channel opening ($C_A \rightarrow O$)? To discriminate between these effects, we examined inactivation from closed states ($C_A \rightarrow I_C$), closed state inactivation (CSI) (Fig. 1). CSI may be viewed as a 'leak' from the activation process. If stretch enhanced the voltage sensitive transitions ($C \rightarrow C_A$) then states C_A would become more populated with stretch. In this scenario, CSI would be enhanced. On the other hand, if stretch affected the gate opening ($C_A \rightarrow O$), channels would be more likely to proceed to opening, thus decreasing the availability of channels in the C_A state. Then, CSI would appear to be decreased.

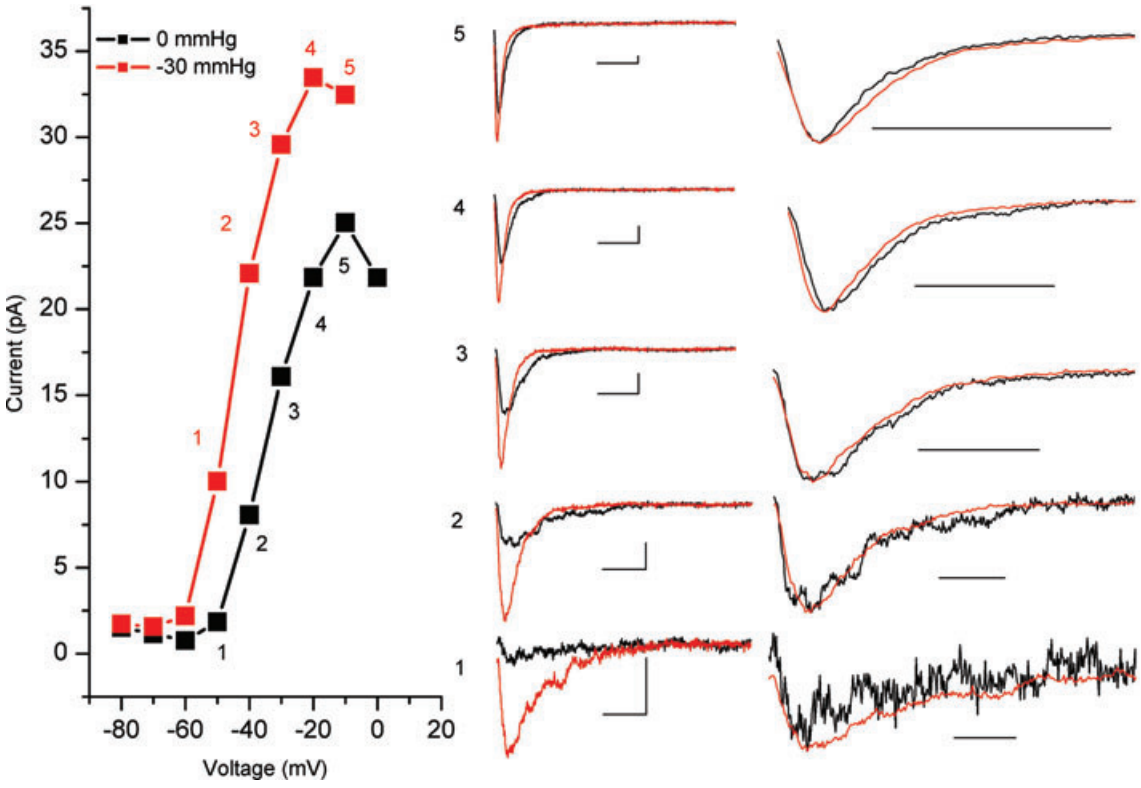

Figure 4. Stretch acceleration of activation and inactivation scales linearly
In the left panel, voltage dependent currents (*I–V*) at 0 mmHg (black) and −30 mmHg (red) are shown. Highlighted points 1–5 track increasing levels of activation. In the middle panel, for the voltage steps marked by 1–5, single time-dependent traces at resting tension (black) are plotted with the corresponding traces for this patch under −30 mmHg stretch (red). In the right panel, traces were normalized to peak current and temporally scaled to times of peak showing that a single time scaling constant accounts for the kinetic changes. Temporal scaling factors (SF) for this patch were 1.57, 1.89, 1.75, 1.47 and 1.71, for points 1–5, respectively.

Closed state inactivation is important at hyperpolarized voltages, where P_o is low and thus channel openings are rare (Armstrong, 2006). At these voltages, the voltage sensors operate, but the channel gates do not yet open. We used a two-step voltage protocol as shown in the top panel of Fig. 5*A*. In the first part of the protocol, after a brief hyperpolarizing pulse and a step back to −140 mV for 5 ms, patches were stepped to 0 mV for 5 ms (Step 1). The same sequence then preceded a step ladder protocol from −140 to −70 mV, with each step lasting 30 ms. Step 2 was a depolarization to 0 mV to assess channel availability. In the bottom left panel of Fig. 5*A* we show a typical set of patch currents. At 0 mmHg (black traces), Step 1 peak currents revealed the maximum available current in the patch at 0 mV (average = 74 ± 2 pA). The following step ladder did not produce currents, signifying that the channels did not activate. Yet, Step 2 peak currents for each step were smaller than the control Step 1 peak. The decrease in peak Step 2 current is proportional to closed state inactivation ($CSI \propto 1 - Step2_{peak}/Step1_{peak}$). For this experiment, $CSI_{0\ mmHg}$ ranged from 0.01 to 0.07 between −140 and −110 mV, meaning that less than 10% of channels inactivated from the closed state. As expected, when this patch was stretched (red traces) Peak 1 and Peak 2 were increased and kinetics accelerated. Also, stretch resulted in some of the ladder steps producing an activating current (−80 and −70 mV), consistent with the negative shift in the voltage dependence of activation. However, the relative increases in Peak 2 currents were significantly smaller than the Peak 1 controls. Under stretch, $CSI_{-30\ mmHg}$ ranged between 0.17 and 0.37 between −140 and −110 mV. The excess CSI due to stretch ($= \Delta CSI = CSI_{0\ mmHg} - CSI_{-30\ mmHg}$) for six patches is shown in Fig. 5*B*. Stretch resulted in an increase in CSI at all voltages but one (−110 mV). Our data show that stretch produced an apparent acceleration of inactivation from closed states. As detailed above, increased CSI with stretch suggests an increased C_A availability secondary to enhanced voltage sensor operation with stretch ($C \rightarrow C_A$).

Recovery from open state inactivation is slower with stretch

We used another two step voltage protocol to test the mechanosensitivity of recovery from open state inactivation (I_O) (Fig. 6*A*, inset). Patches were depolarized to 0 mV for 20 ms (Step 1) to allow fast inactivation to proceed to completion. Step 1 was followed by recovery

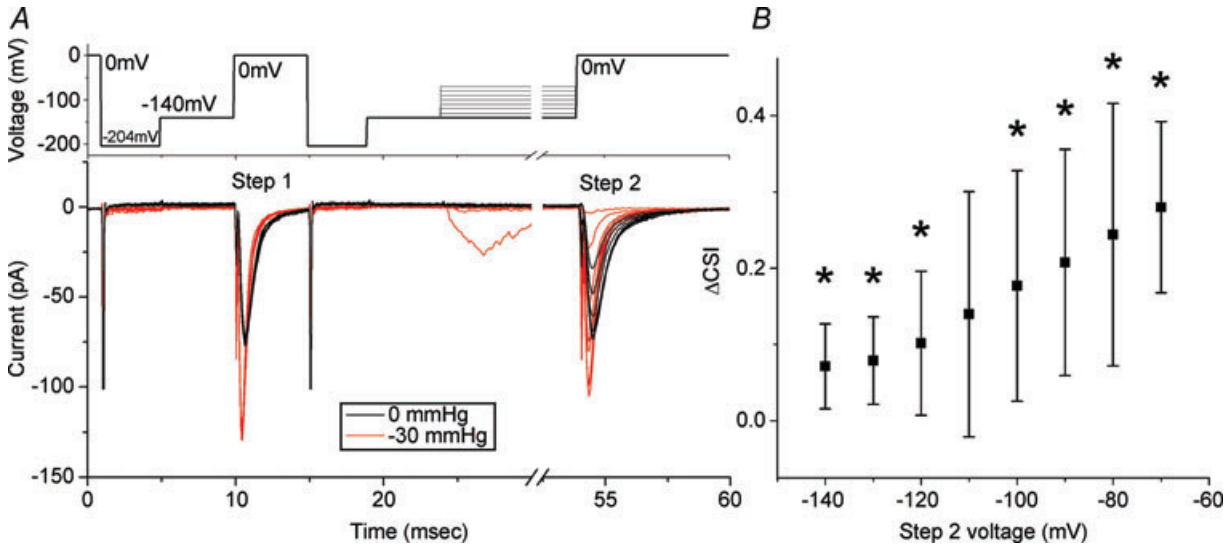

Figure 5. Closed state inactivation (CSI) increases with stretch
A, in the top panel a typical protocol is shown. Prior to both Step 1 and Step 2 patches were stepped through −204 and −140 mV for 4 and 5 ms, respectively. Step 1 was a depolarization to 0 mV for 5 ms, which was followed by a step ladder of 30 ms pulses from −140 to −80 mV and finally a Step 2 depolarization to 0 mV. The bottom panel shows resulting currents for a typical experiment. In black, a patch at resting tension (0 mmHg) has Step 1 and Step 2 peaks that are of nearly identical height. For non-activating Step 2 voltage pulses, the difference in Step 1 and Step 2 peak heights is proportional to closed state inactivation, so $CSI \propto 1 - I_{step2,max}/I_{step1,max,0\ mV}$. For this experiment, $CSI_{0\ mmHg}$ was 0.07, 0.02, 0.01, 0.03, 0.18, 0.35, 0.46 for −140 to −70 mV, respectively. In red, the same patch stretched by a −30 mmHg stimulus has Step 1 peak that is disproportionately larger than Step 2 peak. For this experiment, $CSI_{-30\ mmHg}$ values were 0.22, 0.17, 0.23, 0.37, 0.41, 0.57, for voltages −140 to −90, respectively. Steps to −80 and −70 mV activated small currents and we not include these in the analysis because of open state inactivation. Excess CSI with stretch is $\Delta CSI = CSI_{-30\ mmHg} - CSI_{0\ mmHg}$. For this experiment, ΔCSI was 0.15, 0.16, 0.23, 0.33, 0.34, 0.39 for −140, −130, −120, −110 and −100 mV, respectively. *B*, average ΔCSI for 7 patches plotted against Step 2 voltage. Marked by * are voltages at which stretch resulted in more CSI than no stretch ($p < 0.05$ by t-test).

periods of increasing length (0 to 20 ms) at holding potentials (HP) of −140 through −100 mV. Test current was then elicited by depolarization to 0 mV (Step 2). For a typical experiment at 0 mmHg (Fig. 6*A*, black traces), average Step 1 peak current was 40 ± 2 pA and at HP −120 mV, 16.5 ms was required to reach full recovery by Step 2 current (40 pA). As expected, stretch increased the peak current (44 ± 2 pA) and accelerated the kinetics of the currents evoked by Step 1 (Fig. 6*A*, red traces). Yet, while peak currents of Step 1 increased, the peak currents for Step 2 were smaller than in the non-stretch case and over 20 ms failed to attain full recovery. Recovery of Step 2 peak currents (I_2) was an exponential function of time. Step 2 peaks were normalized to Step 1 peak and fitted to an exponential $I_2/I_1 = I_0 + A(1 - e^{-t/\tau)})$ (Fig. 6*B*). The time constants of recovery from inactivation for resting tension (0 mmHg) and stretched patches (−30 mmHg) were compared as a ratio (τ_{0mm}/τ_{-30mm}) on a patch-by-patch basis and the ratios were then averaged (Fig. 6*C*). At all holding potentials (HPs), recovery was slower for channels that were stretched compared to unstressed channels. The results were statistically significant for all HPs, except −140 mV, where a trend to slower recovery was noted. These findings were not affected by the left-shift of the steady state inactivation curve. At voltages more hyperpolarized than −100 mV, inactivation for even the

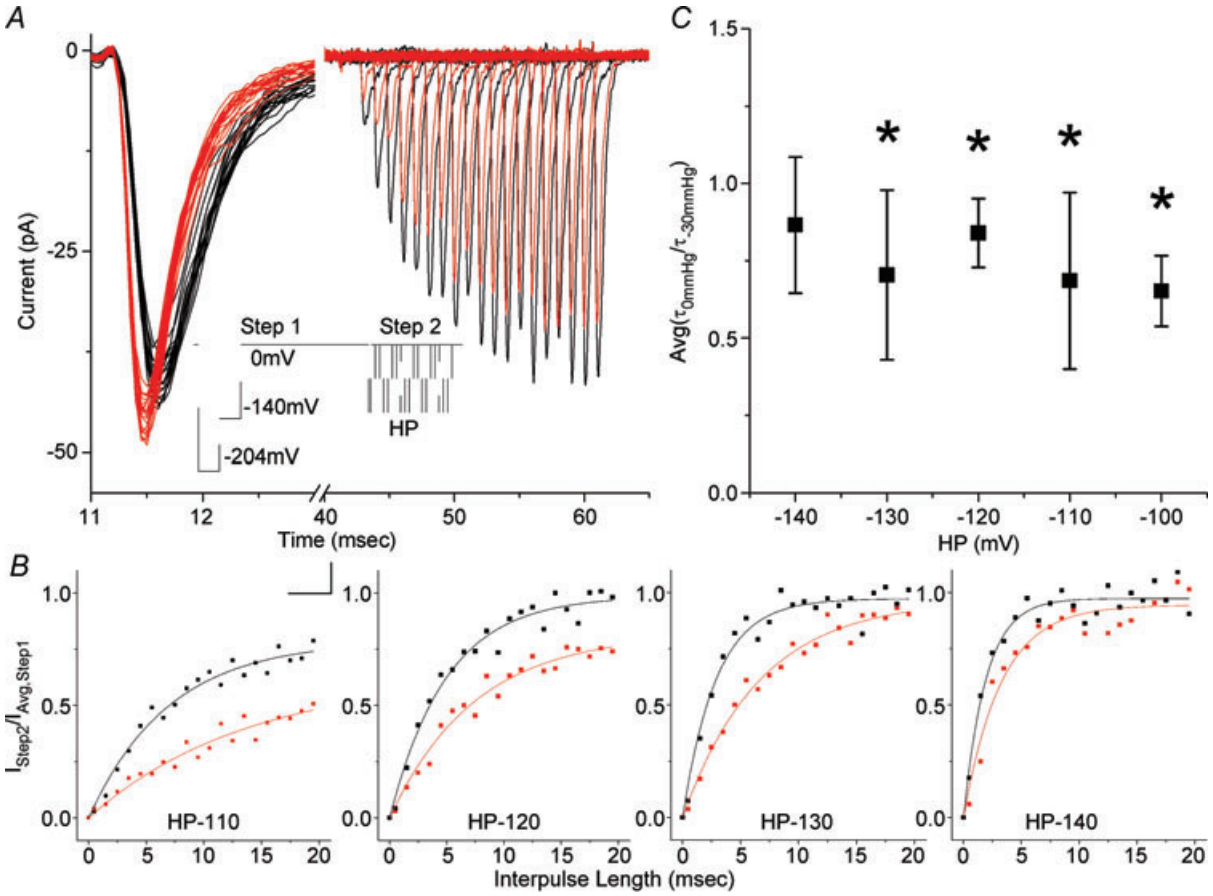

Figure 6. Inactivation recovery is slowed with stretch
A, a two step experiment with a typical protocol is shown in the inset. All protocols had 4 ms long −204 mV and −140 mV steps preceding Step 1 to 0 mV for 20 ms to attain full inactivation. Recovery periods were variable interpulse lengths (0 to 20 ms from 0.5 ms by 1 ms increments) at HP = −140 mV, −130 mV, −120 mV, −110 mV and −100 mV before Step 2 to 0 mV to assess for recovery (scale is 10 ms and 50 mV). Currents in the figure are typical recovery at −120 mV. Stretch resulted in Step 1 current increase and acceleration of kinetics (black is 0 mmHg, red is −30 mmHg). Current inactivated fully over 20 ms Step 1 pulse (first 2 ms shown). Recovery was observed as increasing Step 2 currents. *B*, peak currents from Step 2 were normalized to average Step 1 peak ($I_{Step2}/I_{Avg,Step1}$) and plotted against interpulse length, showing inactivation recovery at resting pressure (0 mmHg, grey) and for a stressed patch (−30 mmHg, black). Data were fitted by an exponential described by $I = I_0 + A(1 - e^{-x/\tau})$. For this experiment, $\tau_{0\ mmHg}$ were 6.0 ± 0.60, 5.1 ± 0.43, 3.1 ± 0.31, 2.3 ± 0.34 ms and $\tau_{-30\ mmHg}$ were 16.0 ± 4.0, 7.4 ± 0.76, 6.8 ± 0.54, 3.4 ± 0.6 ms at HP −110, −120, −130, −140 mV. *C*, recovery from inactivation with stretch relative time constants Avg($\tau_{0\ mmHg}/\tau_{-30\ mmHg}$) as a function of HP voltage at −140 mV ($n = 4$), −130 mV ($n = 4$), −120 mV ($n = 5$), −110 mV ($n = 3$) and −100 mV ($n = 2$).

stretched channels had peaked (Fig. 3*B*), and thus we expected recovery to be unaltered. This slower recovery for stretched channels suggests that the inactivated states are more stable under stretch. The simplest interpretation is that the inactivated states are slightly larger in diameter and/or thinner.

Single channel conductance was unaltered by stretch

The total patch current is $(I) = NiP_o$, where N is the number of channels, i is the single channel current and P_o is the probability of a channel being open. Thus, an increase in total patch current (I) implies an increase in the number of available channels (N), unitary conductance (i) and/or peak open probability (P_o). Single channel records were obtained at a range of pressures and voltages (Fig. 7*A* and *B*). A typical voltage ladder protocol is shown in Fig. 7*A*. Again, we designed this protocol to have a large hyperpolarizing pulse preceding each step to bring channels out of inactivation. In this manner, we were able to collect roughly 200 traces with five steps of voltage from −50 to −10 mV over 30 seconds (overlap shown as grey shadows in Fig. 7*B*). For each voltage step, single channel events were clearly visible after the bulk of the channels in the patch inactivated (Fig. 7*B*). Traces were idealized and single channel events identified using QuB as described in Methods. Figure 7*C* shows a typical all points amplitude histogram for traces at −30 mV for a single patch at rest (0 mmHg, grey) and at −30 mmHg (black). Multiple peaks can be identified on this histogram. The peak around 0 pA is noise, but the other peaks of decreasing height around 1.5 pA, 3.0 pA and 4.5 pA show amplitudes for one, two and three open channels, respectively. The number of events increased with applied pressure, a consistent finding for all patches ($n = 5$). Linear fits ($R = 0.997$) placed the sodium reversal potential at $E_{Na} = +47.9$ mV. Gaussian fits showed the unitary conductance was independent of pressure ($n = 5$) (Fig. 7*B*). The single channel conductance at rest (g_{0mmHg}) was 17.3 ± 0.6 pS, similar to previously published values

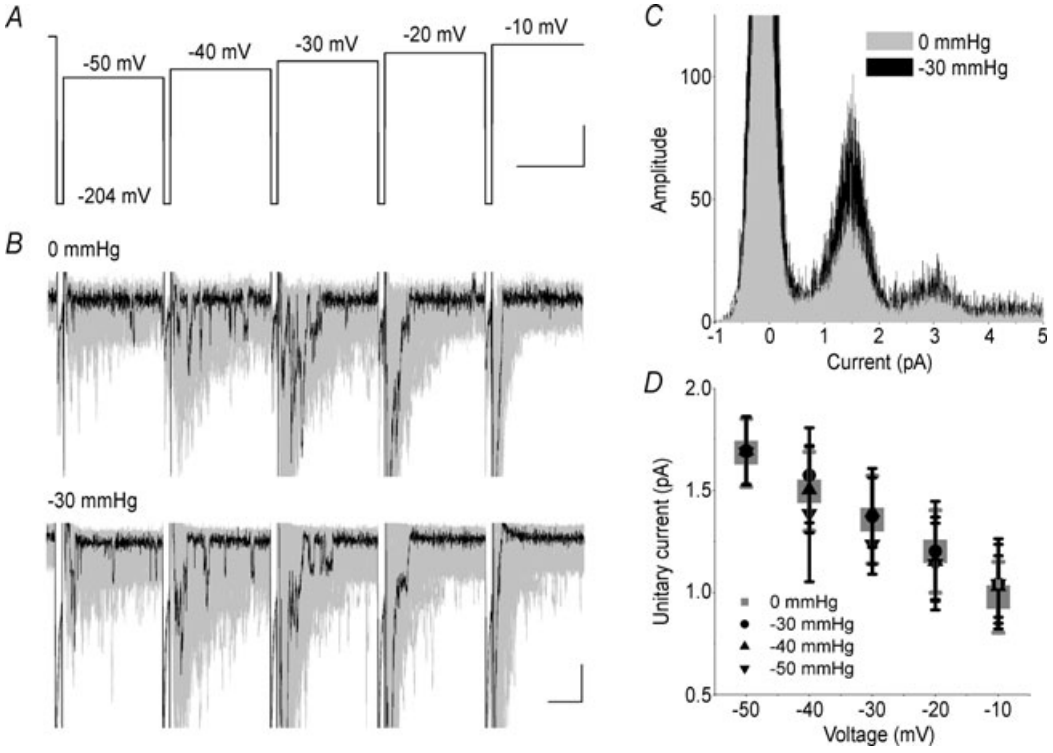

Figure 7. Unitary conductance is not affected by stretch
A, single channel ladder protocol was designed with a 2 ms step to −204 mV, followed by 10 mV steps from −50 mV to −10 mV. To maximize the number of single channel events, 200 ladders were acquired. *B*, typical currents for a patch at rest (0 mmHg) and stretched by a −30 mmHg stimulus. Black highlights a single trace. Grey shadows are overlap of all 200 traces (peaks clipped for display purposes). Segments were then cut to exclude peak activation ($t = 0$ to 6 ms) and single channel events were idealized for subsequent 26 ms. *C*, all points amplitude histogram showing single channel currents at 0 (grey) and −30 mmHg (black) for a typical data set at −30 mV. Amplitude histogram demonstrates qualitative overlap of peaks around 1.5, 3.0 and 4.5 pA for one, two and three channels open, respectively. Amplitude histograms were then fitted with single Gaussians. *D*, average Gauss peaks are plotted against voltage for pressures 0 to −50 mmHg ($n = 5$). Single channel conductances (g) were the same at all pressures, 17.3 ± 0.6, 17.7 ± 0.5, 17.3 ± 0.5, 17.2 ± 0.9, 17.0 ± 0.9, 17.3 ± 0.1 for 0 mmHg, −10 mmHg, −20 mmHg, −30 mmHg, −40 mmHg, −50 mmHg, respectively.

(Hille, 2001), and not significantly different from single channel conductance with stretch (Fig. 7*D*).

Stretch increased the number of active channels in the patch

With unitary conductance (i) not changing, the increases in total patch current (I) are due to an increase in the channel number (N) and/or open probability (P_o). P_o is difficult to estimate for voltage-sensitive Na^+ channels since activation and inactivation overlap in time and P_o does not reach unity. However, the binomial distribution predicts that for a patch with a small number of channels (<5) and $P_o > 0.25$ in 600 depolarizations the likelihood of a single trace with all channels open is $>80\%$. Data from a typical patch are presented in Fig. 8*A*. At rest, this patch had a peak current of 3.12 pA (top panel, red trace) consistent with four channels with a unitary current of $i = 0.78 \pm 0.13$ pA and average current of 0.84 pA, suggesting a P_o of 0.27. When the patch was stretched (bottom panel), peak current increased to 3.79 pA, unitary current was 0.73 ± 0.15 pA and average current rose to 1.0 pA, suggesting a P_o of 0.26, and a channel number of five instead of four. Figure 8*B* shows averaged data for five such patches. The top panel shows that stretched patches had more current at all voltages. The downward slope of these *I–V* curves suggests that maximally stimulating voltage pulses were used, and P_o was maximal. The middle panel shows that there was no significant increase in P_o with stretch, suggesting an increase in the number of channels (lower panel). In the bottom panel, from a starting channel number average of 5.03 ± 0.09, channel number increased by a factor of 1.1 ± 0.4, or $\sim$20%.

Stretch-effects are partially reversible

Reversibility of stretch effects was tracked by measuring the peak current and the shift in voltage dependence of activation over time after removal of the stretch stimulus. Figure 9*A* shows a typical patch for which a -30 mmHg produced a -26 mV shift in $V_{1/2}$ and a 70% increase in peak current. Over the next 5 min $V_{1/2}$ returned to near

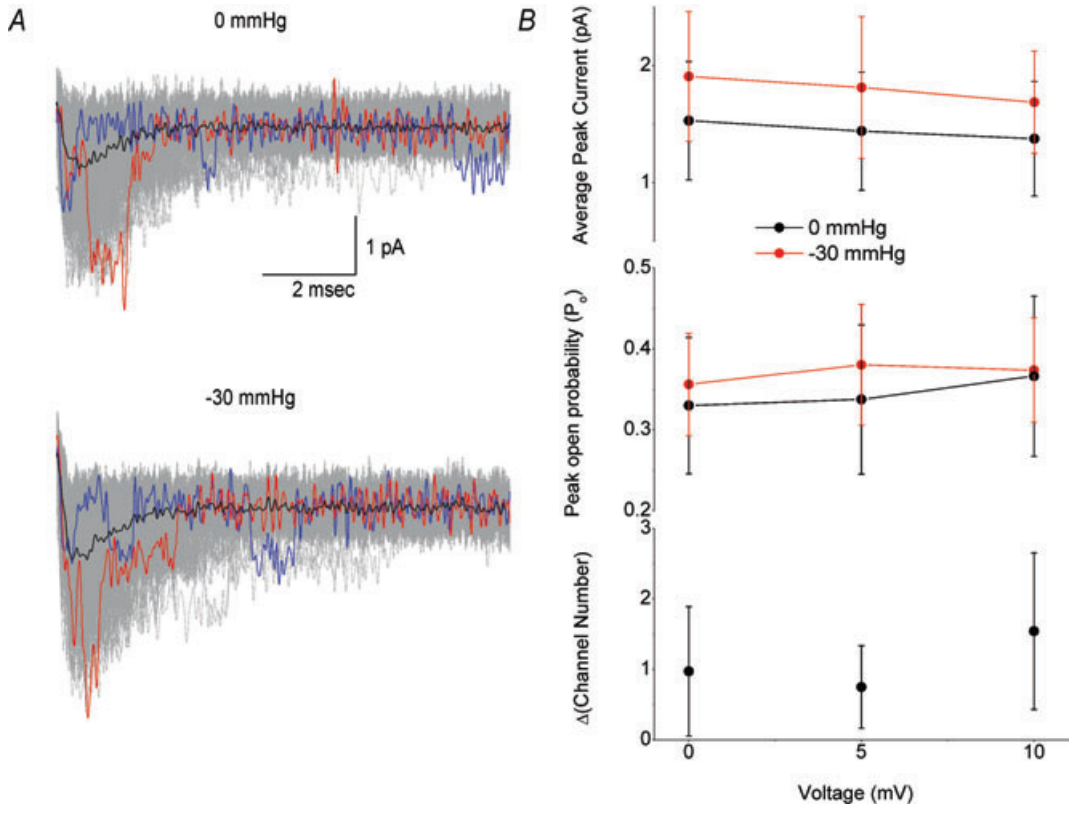

Figure 8. Open probability and channel number in a stretched patch
A, a cell-attached membrane patch was depolarized to 0, +5 and +10 mV. Top panel, at rest (0 mmHg), patch was depolarized to +5 mV, showing single traces (600, grey overlap), the trace with peak amplitude (red), and a trace with resolvable single channel openings (blue) and averaged current (black). Bottom panel, the same patch at −30 mmHg. *B*, top panel, average peak current at 0 mmHg (black) and −30 mmHg (red). Middle panel, max open probability (P_o) at 0 mmHg (black) and −30 mmHg (red). Bottom panel, increase in active channels with stretch (ΔChannel no. = no. channels post – no. channels pre, $n = 5$). No change in P_o was noted but a 23% increase in number of channels was seen.

baseline values while the peak current remained elevated. For all the patches measured using this protocol, a single -30 mmHg stretch produced a $\Delta V_{1/2}$ of -17 ± 6 mV, and recovery was highly variable over the following 5 min, averaging $\Delta V_{1/2} = 4 \pm 10$ mV ($n = 5$) (Fig. 9*B*). Half of the cells returned close to the original baseline, while in two other patches there was a persistent hyperpolarized shift in $V_{1/2}$ even after 30 min. Peak currents also increased with stretch ΔI_{peak} of 31% ($n = 5$). The amplitude of recovery was not uniform, and the peak current remained elevated after 5 min in all but one patch (Fig. 9*C*).

Discussion

The main findings that emerge from this study are that (1) $Na_v1.5$ is mechanosensitive, confirming previous whole cell data (Strege *et al.* 2003*b*) and cell-attached patch results (Morris & Juranka, 2007), (2) stretch produces persistent dose-dependent shifts in the voltage dependence of activation and inactivation due to mechanical modulation of the voltage sensors, and (3) inactivated states are stabilized by stretch. These findings carry physiological and pathophysiological relevance for mechanically active organs where $Na_v1.5$ is expressed.

Patch pressure results in increased tension

The pressures used in this study are routinely attained in organs where $Na_v1.5$ is expressed. The heart and the gut generate and experience pressures in the hundreds of mmHg thousands of times a day. However, at the level of channel function, the relevant parameter is tension, not pressure. Images of the stressed patch showed that suction (≤ -30 mmHg) increased the patch radius of curvature, while maintaining attachment points (Fig. S2). At more elevated pressures, patch creep and loss of stable attachment points were visible for even short stretch stimuli (30 s). Since Laplace's law dictates that $\Delta T = \Delta rP/2$, the increase in patch radius implies an increase in tension, which for a typical stimulus was on the order of 0.01 N m^{-1}. In fact, a distinct advantage of using patches for mechano-stimulation is the well-controlled pressure application of stimulus and a robust response. However, a limitation is that there is poorly controlled resting tension in the patch, as evidenced by an increased variability of voltage sensitivity recorded at rest ($V_{1/2,0\text{mmHg}} \pm 9$ mV), a several-fold increase compared to typical whole-cell measurements. This is in line with previous studies, which have also demonstrated a variable half-point of activation for sodium channels in the cell attached patches over time (Kimitsuki *et al.* 1990) and

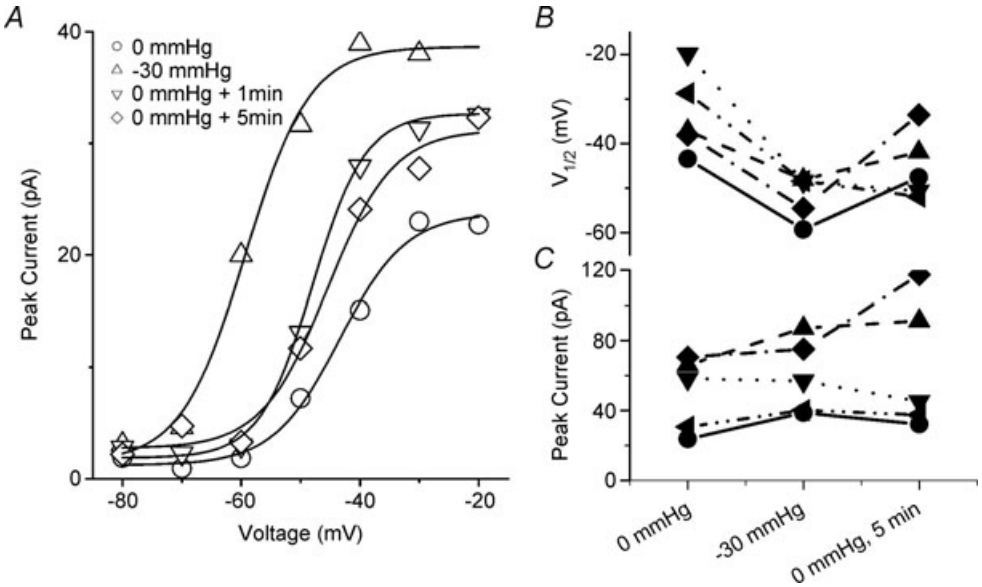

Figure 9. Stretch-induced shift in voltage dependence of activation and the increase in peak current reverse slowly
A, Typical cell attached patch was stretched once by a -30 mmHg pulse for 30 s. *I–V* curves were fitted by a twostate Boltzmann model with the following parameters: at 0 mmHg ($V_{1/2} = -43$ mV, $d_V = 5.6$ mV, $I_{peak} = 23$ pA), -30 mmHg stretch ($V_{1/2} = -59$ mV, dV = 5.4 mV, $I_{peak} = 39$ pA), 0 mmHg + 1 min ($V_{1/2} = -48$ mV, dV = 5.5 mV, $I_{peak} = 33$ pA) and 0 mmHg + 5 min ($V_{1/2} = -45$ mV, dV = 5.5 mV, $I_{peak} = 32$ pA). *B*, In 5 patches, voltage at half-point of activation increased uniformly with stretch, with a variable but incomplete return toward baseline. *C*, Peak current also increased with stretch and in all but one patch remained elevated.

after excision (Fleig *et al.* 1994). This is most likely to be due to baseline mechanical variation of the patch.

Stretch accelerates voltage-dependent activation and stabilizes the inactivated states

Mechanical stress on a patch containing $Na_v1.5$ channels resulted in large hyperpolarizing shifts in voltage dependence of activation and inactivation. This was a robust and striking finding evident for both positive and negative pressures applied to a patch (Fig. 3). Pressure *versus* Boltzmann mid-points of activation and inactivation were linear dose-response fits. The slope of Boltzmann curves did not change significantly (Fig. 3*D*). In previous papers where oocyte patches containing other Na_v channels were stretched, the midpoints of voltage dependence of activation and inactivation were also left-shifted (Shcherbatko *et al.* 1999; Tabarean *et al.* 1999; Wang *et al.* 2009). The current data further show a quantitative dose–response relationship of voltage dependence to pressure, and thus to tension. It is unlikely that these effects were due to artifacts. For example, one may propose that voltage dependence shifts were secondary to increased access resistance for channels residing in the seal (Suchyna *et al.* 2009). This is unlikely for two reasons. First, the slopes of the macroscopic *I–V* curves produced with stretch were not significantly different from those at rest (Fig. 3). Second, increased access resistance should produce a decrease in single channel currents, whereas we observed that single channel amplitudes and Gaussian distributions were not affected with stretch (Fig. 7*C* and *D*).

In the time domain, stretch accelerated both activation and fast inactivation (Fig. 2). This acceleration could be explained by the shift in the voltage half-point of activation. When time-dependent traces were amplitude normalized and temporally scaled, there was good overlap for both activation and inactivation, suggesting a single stretch constant was responsible for the stretch effects (Fig. 4). A recent related study on mechanical effects on the cardiac isoform of $Na_v1.5$ expressed in oocytes also noted the acceleration of activation and inactivation kinetics (Morris & Juranka, 2007). Similarly, an overlap of the time-dependent traces by scaling with a single stretch factor was found. The magnitude of these stretch factors was similar to the ones reported here. Since activation and inactivation are kinetically linked in the gating of the Na_v channels, scaling of the activation and inactivation kinetics by a single constant implies an increase in a single rate constant in the activation sequence of the channel ($C \rightarrow C_A \rightarrow O$). The voltage-dependent steps are prime candidates due to the extensive voltage sensor–lipid interface (Milescu *et al.* 2009), and previous findings of mechanical sensitivity in the oocyte membranes and bilayers (Schmidt & Mackinnon, 2008). However, this is not the only possibility: for example, stabilization of the open state affects the rate-limiting voltage-independent gate opening and can similarly shift the voltage dependence of activation (Zhao *et al.* 2004).

The precise determination of the transitions involved in stretch sensing awaits further single channels studies. Our study provides data that implicate a single transition in the multi-step process of channel activation. Inactivation from closed states increased with pressure (Fig. 5). This fact, in combination with a linear stretch constant and similar size shifts in voltage dependence of both activation and inactivation implies that the acceleration in channel kinetics was due to stretch effects on voltage-dependent transitions and not voltage-independent activation gate opening. The data suggest that $C \rightarrow C_A$ is likely to be responsible for these effects and not $C_A \rightarrow I_A$. Firstly, the shift of steady-state inactivation mirrors the amount of shift in voltage dependence of activation (Figs 3*B* and Fig. 4). Secondly, a separate stretch-sensitive transition in the Na_v gating scheme would prevent simple linear scaling demonstrated in Fig. 4. If a sufficiently large depolarizing stimulus is sustained, channels proceed through the open channel sequence and inactivate by traditional open state inactivation. We found that recovery from the open inactivated state is slowed with stretch, which suggests that pressure stabilizes this inactivated state.

Increase in peak current with stretch is due to an increase in the number of active $Na_v1.5$ channels

Single channel conductance (i) and maximum probability of channel opening (P_o) did not change with stretch (Fig. 8) while estimates of N suggested an increase of about 20% in the number of channels. The conservation of unitary current in the face of increased peak current through the patch is also an important new finding that emerges from this study. The significance of this is that even though $Na_v1.5$ channels can 'sense' mechanical stress, the pores are energetically stable and mechanically protected.

The increase in peak current appears to be a result of an increase in the number of active channels in the patch but the source of this increase is still unclear. Multiple possibilities exist. The first and most obvious is inherent to the patch method. As we have shown above, stretch results in a visible increase in membrane area and a likely alteration of pipette-membrane interface, possibly peeling some of the bilayer off the glass wall and exposing more channels. Both suction (negative pressure) and blowing (positive pressure) may peel the patch from the glass due to the resting tension in the patch (Suchyna *et al.* 2009). Still, we expect less peeling with suction than with blowing. Yet, blowing and suction induced shifts in peak currents

that were identical. For a 30 mmHg positive pressure, peak current increase was 0.32 ± 0.10 ($n = 3$), which compares well to the 30 mmHg suction peak current increase of 0.33 ± 0.10 ($n = 6$). Thus, it is unlikely that simple peeling of the patch membrane is responsible for the increase in peak currents.

A more plausible possibility is that stretch induces an increase in membrane fluidity which allows for an enhanced diffusion of the channels from the seal into the dome of the patch (Oghalai *et al.* 2000). Suchyna *et al.* (2009) have also showed that even at fixed pressure channels can move between the seal and the patch. Mechanical stress was previously shown to change lipid bilayer fluidity and which in turn produced similar shifts in the voltage sensitivity of Na_v channels (Lundbaek *et al.* 2004). The consequence of this in the electromechanical systems may be significant. Mechanical stress is known to be inhomogeneous for cells *in vivo*. Regions of cell membrane with increased fluidity may allow accumulation of channels in those locations. In fact, the asymmetry of $Na_v1.5$ distribution in cardiac myocytes is known, and may be related to mechanical forces (Mazzone *et al.* 2008).

Another explanation may have to do with the possibility of awaking a subset of 'sleepy channels' that are already present in the patch (Matteson & Armstrong, 1982). The authors found that cooling converted some typical Na_V channels into 'sleepy' channels that were slowly activating, but could be aroused by a very positive voltage prepulse. In our system, mechanical stretch inputs energy into the patch, so it may be similar to raising temperature and awaking some of these 'sleepy' channels. The physiological consequence of awaking sleepy channels is also potentially important. Increased density of channels in the areas of increased stretch would result in an inhomogeneous sodium concentration in the cell. In turn, this may affect local calcium concentration and provide feedback for excitation–contraction coupling in the areas of increased mechanical stress (Neco *et al.* 2010).

Stretch of tissues containing $Na_v1.5$ channels may affect physiological function by enhancing activation and allowing a baseline conductance

Alteration of $Na_v1.5$ function or its macromolecular complex components produces disease (Ackerman *et al.* 2004; Locke *et al.* 2006). This channel is found in the heart and gut, two systems in which electromechanical coupling is essential. We show that $Na_v1.5$ is mechanosensitive, but in the strictest sense it is not mechano-activated; it is instead mechano-modulated (Sachs & Morris, 1998). This means that the energy input from mechanical stress is not sufficient to noticeably modulate P_{open} at resting potentials. Instead, we show a large impact of mechanical stimulation on the channel function during channel activation, inactivation and recovery from inactivation. These findings are clearly important for understanding the physiology and pathophysiology of the electromechanical organs.

Contractile organs can be modelled as having a background of steady-state homogeneous stretch, and on this background is superimposed the acute stretch and simultaneous voltage activation. In this setting, we can begin to examine the potential relevance of our findings. Stretch will negatively shift the voltage dependence of activation and inactivation, producing a shift in the window current. We show that the voltage shift is substantial, amounting to tens of millivolts. For the cells that have resting potentials at the window current, this will make them hyperexcitable. The result will be an increase in the baseline current, which has clear implications for pathology, as exemplified in LQT. The Cells that rest at more hyperpolarized potentials will have a larger fraction of channels available for activation, increasing baseline chatter and also making these cells excitable. On the other hand, the cells that rest at more depolarized potentials will have fewer channels available for activation.

The assumption of uniform steady-state stretch is likely to be incorrect. First, at the level of the cell, there are time-dependent changes in stress due to the inhomogeneity of the cytoskeleton (Morone *et al.* 2008) and viscosity of both the cytoskeleton and the bilayer (Suchyna & Sachs, 2007). Our data agree with this notion by showing a prolonged impact of single stretch on channel operation. Second, at the level of mechanically active tissues, steady-state stretch does not hold. These tissues regularly cycle mechanical stimuli and rely on tight mechanoelectrical feedback. The asymmetry of cell surface anatomy and mechanical stress suggests that the notion of a simple shift of window current with stretch is naïve. Instead, the window current will shift in a graded fashion, producing a stretch-dependent distribution of steady state leakage over a wide voltage range. Additionally, with increased underlying activity other channel states will become increasingly important. In this situation the stability of the inactivated states is also paramount. Our results show that stretched channels will preferentially enter the inactivated states from both closed and open states and are likely to require stronger stimuli for further activation. This raises the possibility that mechanical modulation of $Na_v1.5$ is also aimed at protection from out-of-scale mechanical stimuli. Alternatively, cells may use modification of the $Na_v1.5$ cytoskeletal connections (Maruoka *et al.* 2000) and lipid domain (raft) targeting (Tamkun *et al.* 2007) to direct the channel localization and allow normalization of response.

In summary, our data suggest that mechanical stimulation of $Na_v1.5$ results in dose-dependent voltage dependence shifts of activation and inactivation due

to mechanical modulation of the voltage sensors. Our findings suggest that mechanical sensitivity via effects on voltage-dependent channels may play a significant role in the physiology of motile cells.

References

Ackerman MJ (1998). The long QT syndrome: ion channel diseases of the heart. *Mayo Clin Proc* **73**, 250–269.

Ackerman MJ, Splawski I, Makielski JC, Tester DJ, Will ML, Timothy KW, Keating MT, Jones G, Chadha M, Burrow CR, Stephens JC, Xu C, Judson R & Curran ME (2004). Spectrum and prevalence of cardiac sodium channel variants among black, white, Asian, and Hispanic individuals: implications for arrhythmogenic susceptibility and Brugada/long QT syndrome genetic testing. *Heart Rhythm* **1**, 600–607.

Aldrich RW, Corey DP & Stevens CF (1983). A reinterpretation of mammalian sodium channel gating based on single channel recording. *Nature* **306**, 436–441.

Armstrong CM (2006). Na channel inactivation from open and closed states. *Proc Natl Acad Sci U S A* **103**, 17991–17996.

Armstrong CM & Bezanilla F (1977). Inactivation of the sodium channel. II. Gating current experiments. *J Gen Physiol* **70**, 567–590.

Baker PF, Hodgkin AL & Shaw TI (1962). Replacement of the axoplasm of giant nerve fibres with artificial solutions. *J Physiol* **164**, 330–354.

Banderali U, Juranka PF, Clark RB, Giles WR & Morris CE (2010). Impaired stretch modulation in potentially lethal cardiac sodium channel mutants. *Channels (Austin)* **4**, 12–21.

Bennett PB, Yazawa K, Makita N & George AL Jr (1995). Molecular mechanism for an inherited cardiac arrhythmia. *Nature* **376**, 683–685.

Beyder A & Sachs F (2009). Electromechanical coupling in the membranes of Shaker-transfected HEK cells. *Proc Natl Acad Sci U S A* **106**, 6626–6631.

Bezanilla F & Armstrong CM (1977). Inactivation of the sodium channel. I. Sodium current experiments. *J Gen Physiol* **70**, 549–566.

Borjesson SI, Hammarstrom S & Elinder F (2008). Lipoelectric modification of ion channel voltage gating by polyunsaturated fatty acids. *Biophys J* **95**, 2242–2253.

Calabrese B, Tabarean IV, Juranka P & Morris CE (2002). Mechanosensitivity of N-type calcium channel currents. *Biophys J* **83**, 2560–2574.

Caldwell RA, Clemo HF & Baumgarten CM (1998). Using gadolinium to identify stretch-activated channels: technical considerations. *Am J Physiol Cell Physiol* **275**, C619–621.

Elinder F & Arhem P (1994). Effects of gadolinium on ion channels in the myelinated axon of *Xenopus laevis*: four sites of action. *Biophys J* **67**, 71–83.

Farrugia G, Holm AN, Rich A, Sarr MG, Szurszewski JH & Rae JL (1999). A mechanosensitive calcium channel in human intestinal smooth muscle cells. *Gastroenterology* **117**, 900–905.

Fleig A, Ruben PC & Rayner MD (1994). Kinetic mode switch of rat brain IIA Na channels in *Xenopus* oocytes excised macropatches. *Pflugers Arch* **427**, 399–405.

Gellens ME, George AL Jr, Chen LQ, Chahine M, Horn R, Barchi RL & Kallen RG (1992). Primary structure and functional expression of the human cardiac tetrodotoxin-insensitive voltage-dependent sodium channel. *Proc Natl Acad Sci U S A* **89**, 554–558.

Gil Z, Silberberg SD & Magleby KL (1999). Voltage-induced membrane displacement in patch pipettes activates mechanosensitive channels. *Proc Natl Acad Sci U S A* **96**, 14594–14599.

Gu CX, Juranka PF & Morris CE (2001). Stretch-activation and stretch-inactivation of Shaker-IR, a voltage-gated K^+ channel. *Biophys J* **80**, 2678–2693.

Hille B (2001). *Ion Channels of Excitable Membranes*. Sinauer Associates, Inc., Sunderland, MA.

Horn R (1991). Estimating the number of channels in patch recordings. *Biophys J* **60**, 433–439.

Jiang Y, Lee A, Chen J, Ruta V, Cadene M, Chait BT & MacKinnon R (2003). X-ray structure of a voltage-dependent K^+ channel. *Nature* **423**, 33–41.

Kimitsuki T, Mitsuiye T & Noma A (1990). Negative shift of cardiac Na^+ channel kinetics in cell-attached patch recordings. *Am J Physiol Heart Circ Physiol* **258**, H247–254.

Kraichely RE, Strege PR, Sarr MG, Kendrick ML & Farrugia G (2009). Lysophosphatidyl choline modulates mechanosensitive L-type Ca^{2+} current in circular smooth muscle cells from human jejunum. *Am J Physiol Gastrointest Liver Physiol* **296**, G833–839.

Laitko U, Juranka PF & Morris CE (2006). Membrane stretch slows the concerted step prior to opening in a Kv channel. *J Gen Physiol* **127**, 687–701.

Laitko U & Morris CE (2004). Membrane tension accelerates rate-limiting voltage-dependent activation and slow inactivation steps in a Shaker channel. *J Gen Physiol* **123**, 135–154.

Locke GR 3rd, Ackerman MJ, Zinsmeister AR, Thapa P & Farrugia G (2006). Gastrointestinal symptoms in families of patients with an SCN5A-encoded cardiac channelopathy: evidence of an intestinal channelopathy. *Am J Gastroenterol* **101**, 1299–1304.

Lundbaek JA, Birn P, Hansen AJ, Sogaard R, Nielsen C, Girshman J, Bruno MJ, Tape SE, Egebjerg J, Greathouse DV, Mattice GL, Koeppe RE 2nd & Andersen OS (2004). Regulation of sodium channel function by bilayer elasticity: the importance of hydrophobic coupling. Effects of Micelle-forming amphiphiles and cholesterol. *J Gen Physiol* **123**, 599–621.

Lyford GL & Farrugia G (2003). Ion channels in gastrointestinal smooth muscle and interstitial cells of Cajal. *Curr Opin Pharmacol* **3**, 583–587.

Makielski JC, Ye B, Valdivia CR, Pagel MD, Pu J, Tester DJ & Ackerman MJ (2003). A ubiquitous splice variant and a common polymorphism affect heterologous expression of recombinant human SCN5A heart sodium channels. *Circ Res* **93**, 821–828.

Maruoka ND, Steele DF, Billie PY, Dan P, Zhang X, Moore EDW & Fedida D (2000). α-Actinin-2 couples to cardiac Kv1.5 channels, regulating current density and channel localization in HEK cells. *FEBS Lett* **473**, 188–194.

Matteson DR & Armstrong CM (1982). Evidence for a population of sleepy sodium channels in squid axon at low temperature. *J Gen Physiol* **79**, 739–758.

Mazzone A, Strege PR, Tester DJ, Bernard CE, Faulkner G, De Giorgio R, Makielski JC, Stanghellini V, Gibbons SJ, Ackerman MJ & Farrugia G (2008). A mutation in telethonin alters Nav1.5 function. *J Biol Chem* **283**, 16537–16544.

Milescu M, Bosmans F, Lee S, Alabi AA, Kim JI & Swartz KJ (2009). Interactions between lipids and voltage sensor paddles detected with tarantula toxins. *Nat Struct Mol Biol* **16**, 1080–1085.

Morone N, Nakada C, Umemura Y, Usukura J & Kusumi A (2008). Three-dimensional molecular architecture of the plasma-membrane-associated cytoskeleton as reconstructed by freeze-etch electron tomography. *Methods Cell Biol* **88**, 207–236.

Morris CE & Juranka PF (2007). Nav channel mechanosensitivity: activation and inactivation accelerate reversibly with stretch. *Biophys J* **93**, 822–833.

Morris CE, Juranka PF, Lin W, Morris TJ & Laitko U (2006). Studying the mechanosensitivity of voltage-gated channels using oocyte patches. *Methods Mol Biol* **322**, 315–329.

Neco P, Rose B, Huynh N, Zhang R, Bridge JH, Philipson KD & Goldhaber JI (2010). Sodium-calcium exchange is essential for effective triggering of calcium release in mouse heart. *Biophys J* **99**, 755–764.

Oghalai JS, Zhao HB, Kutz JW & Brownell WE (2000). Voltage- and tension-dependent lipid mobility in the outer hair cell plasma membrane. *Science* **287**, 658–661.

Opsahl LR & Webb WW (1994). Lipid-glass adhesion in giga-sealed patch-clamped membranes. *Biophys J* **66**, 75–79.

Ou Y, Strege P, Miller SM, Makielski J, Ackerman M, Gibbons SJ & Farrugia G (2003). Syntrophin $\gamma 2$ regulates SCN5A gating by a PDZ domain-mediated interaction. *J Biol Chem* **278**, 1915–1923.

Qin F (2004). Restoration of single-channel currents using the segmental k-means method based on hidden Markov modeling. *Biophys J* **86**, 1488–1501.

Qin F, Auerbach A & Sachs F (1996). Estimating single-channel kinetic parameters from idealized patch-clamp data containing missed events. *Biophys J* **70**, 264–280.

Sachs F & Morris CE (1998). Mechanosensitive ion channels in nonspecialized cells. *Rev Physiol Biochem Pharmacol* **132**, 1–77.

Saito YA, Strege PR, Tester DJ, Locke GR 3rd, Talley NJ, Bernard CE, Rae JL, Makielski JC, Ackerman MJ & Farrugia G (2009). Sodium channel mutation in irritable bowel syndrome: evidence for an ion channelopathy. *Am J Physiol Gastrointest Liver Physiol* **296**, G211–218.

Schmidt D & Mackinnon R (2008). Voltage-dependent K^+ channel gating and voltage sensor toxin sensitivity depend on the mechanical state of the lipid membrane. *Proc Natl Acad Sci U S A* **105**, 19276–19281.

Shcherbatko A, Ono F, Mandel G & Brehm P (1999). Voltage-dependent sodium channel function is regulated through membrane mechanics. *Biophys J* **77**, 1945–1959.

Strege PR, Holm AN, Rich A, Miller SM, Ou Y, Sarr MG & Farrugia G (2003*a*). Cytoskeletal modulation of sodium current in human jejunal circular smooth muscle cells. *Am J Physiol Cell Physiol* **284**, C60–66.

Strege PR, Ou Y, Sha L, Rich A, Gibbons SJ, Szurszewski JH, Sarr MG & Farrugia G (2003*b*). Sodium current in human intestinal interstitial cells of Cajal. *Am J Physiol Gastrointest Liver Physiol* **285**, G1111–1121.

Suchyna TM, Markin VS & Sachs F (2009). Biophysics and structure of the patch and the gigaseal. *Biophys J* **97**, 738–747.

Suchyna TM & Sachs F (2007). Mechanosensitive channel properties and membrane mechanics in mouse dystrophic myotubes. *J Physiol* **581**, 369–387.

Tabarean IV, Juranka P & Morris CE (1999). Membrane stretch affects gating modes of a skeletal muscle sodium channel. *Biophys J* **77**, 758–774.

Tamkun MM, O'Connell K M & Rolig AS (2007). A cytoskeletal-based perimeter fence selectively corrals a sub-population of cell surface Kv2.1 channels. *J Cell Sci* **120**, 2413–2423.

Wang JA, Lin W, Morris T, Banderali U, Juranka PF & Morris CE (2009). Membrane trauma and Na^+-leak from Nav1.6 channels. *Am J Physiol Cell Physiol* **297**, C823–834.

Zhao Y, Yarov-Yarovoy V, Scheuer T & Catterall WA (2004). A gating hinge in Na^+ channels: a molecular switch for electrical signaling. *Neuron* **41**, 859–865.

Author contributions

The authors approved the final version. This work was performed in the laboratory of Gianrico Farrugia, Mayo Clinic, Rochester, MN, USA. Conception and design of the experiments: A.B., J.L.R., C.B., G.F.; collection, analysis and interpretation of data: A.B., J.L.R., C.B., P.R.S., G.F.; drafting the article or revising in critically for important intellectual content: A.B., J.L.R., F.S., G.F.

Acknowledgements

The authors would like to thank Drs Lorin Milescu, Thomas Suchyna and Catherine Morris for valuable discussions and comments on the manuscript. This work was supported by The National Institute of Diabetes and Digestive and Kidney Diseases (NIDDK) R01 52766.